Flow-to-fracture transition in a volcanic mush plug may govern normal eruptions at Stromboli

J. Suckale[1], T Keller[1], K V Cashman[2,3], P-O Persson[4]

[1]Department of Geophysics, Stanford University, 397 Panama Mall, Stanford, CA-94305, USA.

[2]School of Earth Sciences, University of Bristol, Wills Memorial Building, Queen's Road, Bristol BS8 1RJ, UK.

[3]Department of Geological Sciences, University of Oregon, 1272 University of Oregon, Eugene, OR-97403, USA

[4]Department of Mathematics, University of California, Berkeley, 970 Evans Hall, Berkeley, CA-94720, USA.

Corresponding author: Jenny Suckale (jsuckale@stanford.edu)

Key Points:

- Rheological transition in crystalline magma creates a porous mush plug beneath Strombolian crater terrace.
- Localized gas segregation may give rise to hot conduits of high gas flux and mobile magma through the volcanic plug.
- Strombolian eruptions may be result of a flow-to-fracture transition in the mush plug induced by crustal stresses and gas over-pressure.

Abstract

Stromboli is a model volcano for studying eruptions driven by degassing. The current paradigm posits that Strombolian eruptions represent the bursting of gas slugs ascending through melt-filled conduits, but petrological observations show that magma at shallow depth is crystalline enough to form a three-phase plug consisting of crystals, bubbles and melt. We combine a 1D model of gas flushing a crystalline mush with a 3D stress model. Our results suggest that localized gas segregation establishes hot conduits of mobile magma within a stagnant plug. The plug is prone to tensile failure controlled by gas over-pressure and tectonic stress, with failure most likely beneath the observed vent locations. We hence argue that Strombolian eruptions are related to plug failure rather than flow. Our proposed three-phase model of the shallow plumbing system may provide a promising framework for integrating geophysical, petrological and morphological observations at Stromboli, and in open-system volcanism more generally.

1. Introduction

Stromboli volcano in Italy is best known for its episodic "normal" activity, defined as discrete explosive bursts that last tens of seconds and eject pyroclasts to a height of 100-200 m [*Barberi et al.*, 1993]. Normal explosions are driven by gas, as evidenced by the high proportion of erupted gas relative to magma [*Allard et al.*, 1994], and the observation that high gas fluxes are associated with more frequent and more vigorous eruptions than low gas fluxes [*Colò et al.*, 2010; *Taddeucci et al.*, 2013]. The leading paradigm [*Blackburn et al.*, 1976] posits that normal eruptions at Stromboli and other volcanoes (e.g. [*Vergniolle and Mangan*, 2000]) represent the buoyant ascent and burst of a large conduit-filling gas bubble, commonly referred to as a slug, through a pipe-shaped conduit filled with magma (Fig. 1A). The goal of this paper is to generalize this view of normal eruptions as a two-phase process involving gas and melt to a three-phase framework by integrating the role of crystals. In addition to considering viscous flow, we evaluate the effects a more complex magma rheology including the possibility of magma failure (Fig. 1B).

Idealized laboratory experiments of three-phase aggregates show that adding solid particles to a viscous liquid creates a wide spectrum of multi-phase interactions. These depend on the relative importance of liquid viscosity, gas compressibility, and inter-particle friction [*Knudsen et al.*, 2008; *Sandnes et al.*, 2011]. An increasing solid fraction causes the rheology of the mixture to stiffen, leading to behavior similar to gas percolating through a porous solid [*Chevalier et al.*, 2008, 2009]. As the aggregate strength increases it may undergo a flow-to-fracture transition [*Shin and Santamarina*, 2010; *Varas et al.*, 2010, 2013; *Holtzman et al.*, 2012; *Islam et al.*, 2013]. This causes a significant increase in the efficiency of gas and/or liquid segregation, highlighting its potential importance for understanding volcanic eruptions.

Here, we propose that highly crystalline magma in the shallow Strombolian plumbing system behaves as a type of volcanic plug. It differs from plugs proposed for more silicic volcanic systems [*Marsh*, 2000] in that it is porous enough to allow continuous degassing. Thus, over-pressure build-up beneath the plug does not typically exceed the threshold for catastrophic failure. Paroxysmal eruptions are the exception to this rule, but our focus here is on understanding normal Strombolian activity. We propose a model where localized gas segregation through a stagnant mush plug gives rise to hot pathways filled with mobile magma. These dynamically established conduits accommodate the majority of gas flux through the system. Gas pore pressure in combination with edifice-scale stress distribution can lead to magma failure at the head of some degassing pulses, which thus accelerate to form normal eruptions.

2. Observational constraints from petrology, geophysics and morphology

Petrological data gives the clearest evidence for the presence of a mush plug in the Strombolian plumbing system. The uppermost few hundred meters are composed of highly porphyritic (HP), water-poor (<0.5 wt%) magma with 45-60 vol% phenocrysts and micro-phenocrysts that is erupted as scoria during normal activity [*Métrich et al.*, 2001; *Francalanci et al.*, 2004, 2005]. Low-porphyritic (LP), water-rich (>2.5 wt%) magma with <10 vol.% phenocrysts originates much deeper (~3 km) and is ejected as pumice only during major eruptions, alongside scoria bearing the characteristics of HP magma [*Métrich et al.*, 2001; *Bertagnini et al.*, 2003; *Francalanci et al.*, 2004, 2005]. Experimental data [*Conte et al.*, 2006; *Agostini et al.*, 2013] point to rapid crystallization of plagioclase around 10 MPa, or 400-600 m depth depending on density. The rapid increase in crystallinity should translate into a rheological transition from a mobile viscous liquid to a stagnant plug [*Arzi*, 1978; *van der Molen and Paterson*, 1979; *Renner et al.*, 2000a; *Gurioli et al.*, 2014].

Geomorphological and geophysical data offer a variety of constraints in addition to petrology. The eruptive center at Stromboli consists of three distinct features: the crater terrace, the craters and the vents (Fig. 1B). The crater terrace is an approximately elliptical area near the summit of the volcano measuring about 280 m by 150 m. It is composed of three main craters that are tens of meters in size, located in the North-East (NE), central, and South-West (SW) portion of the crater terrace. This three-crater geometry can be traced back to at least 1776 [*Washington*, 1917] and appears to be surprisingly stable; for example, it was re-established only months after the crater terrace collapsed during the effusive eruption in 2002-2003 [*Calvari et al.*, 2005; *Ripepe et al.*, 2005b]. The craters typically contain several vents, each a few meters across, which may accommodate both continuous gas "puffing" as well as magma ejection during normal eruptions. Both the location and number of active vents within the craters vary over time scales of months [*Harris et al.*, 1996; *Harris and Ripepe*, 2007a].

Geophysical data suggest that surface vents are linked to a common gas source a few hundred meters below the craters [*Kirchdörfer*, 1999; *Wielandt and Forbriger*, 1999; *Genco and Ripepe*, 2010]. This is evidenced by correlations in the number of eruptions at different vents [*Settle and McGetchin*, 1980], thermal mapping of the crater terrace [*Harris et al.*, 1996], and coupled thermal oscillations at different craters [*Ripepe et al.*, 2005a]. Self-potential surveys and tracking of gas anomalies further point towards convective cells consisting of gas and dense magmatic liquid beneath the entire crater terrace [*Ballestracci*, 1982; *Finizola et al.*, 2003]. These data suggest that a convective reservoir underlies a plug of HP magma mush that extends beneath the entire crater terrace (Fig. 1B). This interpretation is consistent with depressurization cycles in the upper 300-800 m inferred from seismic and strain-meter data [*De Martino et al.*, 2012], and with temporal variations in the amplitude of high-frequency gravity [*Carbone et al.*, 2012]. The petrology, morphology and geophysics of Stromboli are all consistent with the existence of a shallow porous plug containing dynamically emerging volcanic conduits located beneath the crater terrace.

3. Volcanic plug model

Degassing and crystallization from pressure-dependent dehydration likely govern the properties of the upper plumbing system [*Landi et al.*, 2004; *Métrich et al.*, 2009]. As hydrated magma ascends it becomes saturated in water and re-equilibrates by exsolving water into a vapor phase while crystallizing plagioclase. To characterize the properties of the hypothesized volcanic plug at Stromboli, we construct a one-dimensional, steady-state model of dehydration, crystallization and gas segregation through a three-phase magma mush. The model represents the top 1 km of the Strombolian plumbing system. Our setup implies that the deeper magma processing system provides a steady flux of well-mixed magma with approximately constant temperature, water content, and crystallinity into this shallow part of the plumbing system.

Phase proportions in the model are functions of pressure, temperature and water content similar to *La Spina et al.* [2015]. We define volume fractions ϕ_x for silicate crystals (solid phase), ϕ_m for silicate melt (liquid phase), and ϕ_v for water vapor (gas phase). We define the gas fraction as proportional to the difference between the melt water content supplied at depth $D = 1$ km, X^0_{H2O}, and the pressure-dependent saturated water content of the melt, $X^{\mathrm{sat}}_{\mathrm{H2O}}(P)$:

$$\phi_v = \phi_v^0 + (\phi_v^{\max} - \phi_v^0)\left(\frac{X^{\mathrm{sat}}_{\mathrm{H2O}}(P) - X^0_{\mathrm{H2O}}}{X^{\mathrm{atm}}_{\mathrm{H2O}} - X^0_{\mathrm{H2O}}}\right) . \quad (1)$$

The two parameters controlling the vesicularity profile are hence the gas fraction of magma at depth, ϕ_v^0, and the maximum vesicularity reached at the surface of the model column, ϕ_v^{max}. The saturation profile with pressure is a 4th order polynomial fit to the calculated values in *Cigolini et al.*, [2015], Table A4. The melt fraction, ϕ_m, is a function of the homologous temperature [e.g., *Katz*, 2003]:

$$\phi_m = (1 - \phi_v)\left(\frac{T - T_{\mathrm{sol}}}{T_{\mathrm{liq}} - T_{\mathrm{sol}}}\right)^{1.75}, \qquad (2)$$

where the first factor compensates for the independently set vesicularity, and the solidus (T_{sol}) and liquidus (T_{liq}) temperatures are decreasing functions of $X_{\mathrm{H2O}}^{\mathrm{sat}}(P)$:

$$T_{\mathrm{sol}} = T_{\mathrm{sol}}^0 - \Delta T_{\mathrm{sol}} \times X_{\mathrm{H2O}}^{\mathrm{sat}}(P)\ , \qquad (3a)$$

$$T_{\mathrm{liq}} = T_{\mathrm{liq}}^0 - \Delta T_{\mathrm{liq}} \times X_{\mathrm{H2O}}^{\mathrm{sat}}(P)\ . \qquad (3b)$$

The dry solidus and liquidus at ambient conditions are $T_{\mathrm{sol}}^0 = 900$°C, and $T_{\mathrm{liq}}^0 = 1250$ °C. The water-dependent factors $\Delta T_{\mathrm{sol}} = 200$ °C/wt%, and $\Delta T_{\mathrm{sol}} = 100$ °C/wt% are somewhat exaggerated to emphasize the effect of dehydration. Finally, we infer the crystallinity from

$$\phi_x = 1 - \phi_m - \phi_v\ . \qquad (4)$$

The pressure *P* is lithostatic and computed based on the aggregate density $\bar{\rho} = \sum \phi_i \rho_i$, which depends on phase densities, ρ_i, and their relative fractions. We set the melt density to 2700 kg m^{-3}. The solid density depends on the crystallizing mineral phases, which we set to 3300 kg m^{-3} for the initial crystal content at depth (plagioclase, clinopyroxene and olivine), and 2700 kg m^{-3} for the crystal content added during dehydration (mostly plagioclase). The density of the vapor phase is that of an ideal gas and hence depends on pressure.

We approximate the rheological transition occurring between a melt-supported and a crystal-supported aggregate with a hyperbolic tangent function in logarithmic space fixed at a critical crystallinity, $\phi_x^{\text{crit}} = 0.5$, motivated by [*Renner et al.*, 2000b; *Caricchi et al.*, 2007; *Pistone et al.*, 2013]. The mush viscosity also depends on temperature according to an Arrhenius law, and on water content in the melt $X_{\text{H2O}}^{\text{sat}}$ as a log-linear variation [e.g., *Cigolini et al.*, 2008] (see SI for details).

We assume buoyancy-driven Darcy flow through a static porous matrix to estimate the vertical percolation speed of gas, u:

$$u = \frac{k}{\phi_v \mu}(\bar{\rho} - \rho_v)g \, , \tag{5}$$

where the permeability of Strombolian lava follows a 5th order power-law of the vesicularity, $k = 6\times10^{-11}\ \text{m}^2 \phi_v^5$, as estimated specifically for Strombolian lava [*Bai et al.*, 2010]. The gas viscosity is constant at $\mu = 5\times10^{-6}$ Pa s. The flow of gas through the magma mush provides advective heat transport, which competes with conductive heat loss towards the cool surface of the volcano. Assuming thermal equilibrium between phases the conservation of energy is

$$\frac{\partial T}{\partial t} + \frac{\phi_v \rho_v}{\bar{\rho}} u \cdot \frac{\partial T}{\partial z} = \kappa \frac{\partial^2 T}{\partial z^2} + \frac{4\kappa}{D^2}(T_c - T) \, . \tag{6}$$

The second term on the right hand side is the simplified contribution of lateral heat loss towards the cooler edifice surrounding the mush column, with T_c the crustal geotherm, z the depth coordinate, and $D = 1$ km. The thermal conductivity is constant at $\kappa = 10^{-6}\ \text{m}^2$. We solve for the phase fractions, the mush density and viscosity, and, u and T by a standard fixed-point iterative scheme, resolving non-linearities to a relative tolerance of 10^{-9} (see SI for details and code access).

Darcy flow through a viscous matrix has an inherent physical length scale δ, known as the compaction length [*McKenzie*, 1984], over which an interconnected pore space may be established. In the case of gas percolating through a magmatic mush matrix, δ depends on the viscosity of the magma and the vapor, as well as the permeability and vesicularity of the mush:

$$\delta = \sqrt{\frac{\eta\, k(\phi_v)}{\phi_v\, \mu}}\,. \tag{8}$$

This scale may vary significantly (~0.1–100 m) within a volcanic mush. Scaling analysis further states that the percolating phase (i.e., the water vapor) builds up a characteristic pressure difference ΔP to the matrix (i.e., the crystalline mush) at the head of each interconnected pulse:

$$\Delta P = P_v - P_{\mathrm{mush}} \sim \Delta\rho g \delta\ , \tag{7}$$

with P_{mush} the pressure in the mush, and $\Delta\rho = \rho_{\mathrm{mush}} - \rho_v$ the density difference between mush and vapor.

Griffith theory of failure by tensile micro-cracking suggests that the limited tensile strength, T_0, of the magma mush imposes an upper limit on this pressure difference. If that failure criterion is reached, the magma fractures locally at the head of the gas pulse. This process can significantly accelerate gas ascent and lead to an eruption. The failure criterion is

$$\tau^2 = 4T_0\,(P_{\mathrm{eff}} + T_0) \tag{9}$$

where $\tau = \sqrt{2\,\sigma_{II}}$ represents the shear stress magnitude computed from the second invariant of the deviatoric stress tensor, σ_{II} , and the effective pressure P_{eff} [*Skempton*, 1960] is defined as the difference between the mean normal stress or pressure in the three-phase mixture, $\bar{P}$, and the pore pressure, P_v, which relates it to the pressure difference ΔP as

$$P_{\mathrm{eff}} = \bar{P} - P_v = -(1-\phi_v)\Delta P. \tag{10}$$

To quantitatively assess whether tensile failure of the magmatic mush is likely to occur at Stromboli, we complement the 1D mush column model with a 3D mechanical model. We assume that the plug is approximately homogeneous (see SI) and characterized by a finite yield strength, as suggested by both infrasonic measurements [*Ripepe et al.*, 2007] and rheological experiments [*Gurioli et al.*, 2014]. Yield strength in three-phase mushes arises from jamming, which results from the presence of force chains between closely packed particles [*Liu and Nagel*, 2010; *Majmudar and Behringer*, 2005]. Yielding occurs as grain-grain contacts become mobilized, but contrary to brittle failure in competent rocks, yielding merely leads to short-term fluctuations around a relatively constant finite stress governed by external forcing instead of relieving the accumulated potential energy entirely [*Tordesillas*, 2007]. To estimate the time-averaged state of stress inside the plug from topography, tectonics and material differences, we model the plug as a weak body embedded in an elastic edifice,

$$\nabla \cdot \boldsymbol{\sigma}(\boldsymbol{x}) + \bar{\rho}(\boldsymbol{x})\boldsymbol{g} = 0 \,, \tag{11}$$

where $\boldsymbol{\sigma}(\boldsymbol{x})$ is the stress tensor, $\bar{\rho}(\boldsymbol{x})$ the bulk density, $\boldsymbol{g}$ the gravity vector, and $\boldsymbol{x}$ the coordinate vector. We solve for the stress in the plug using a standard finite element method [*Peraire and Persson*, 2011] and assume that the main direction of extension strikes SE–NW as evidenced by normal faults in the proximity of Stromboli trending SW–NE [*Tibaldi et al.*, 2003; *Montone et al.*, 2012]. We assume that the shear modulus of the plug is one to two orders of magnitude smaller than the edifice rock and can hence only sustain stresses of similar magnitude as the yield strength.

4. Results

Non-explosive degassing is the dominant mode of gas extraction at Stromboli [*Allard et al.*, 1994], implying that the upper plumbing system is continually flushed by hot gas. The percolating gas is likely subject to several localization instabilities [e.g., *Saffman and Taylor*, 1958; *Stevenson*, 1989; *Aharonov et al.*, 1995; *Spiegelman et al.*, 2001; *Keller and Katz*, 2016], which are amplified by the pronounced power-law relationship between permeability and gas content at Stromboli [*Bai et al.*, 2010], the strong dependence of the melt water saturation point on pressure, and the expansion of gas under decompression.

Mechanically, degassing weakens the magmatic mush if percolating gas bubbles act as Griffith flaws that help to facilitate tensile failure [e.g., *Oppenheimer et al., 2015*]. Thermally, a sufficient gas percolation speed maintains a high temperature along degassing pathways. To quantify the relative importance of heat transport to diffusion, we estimate the Péclet number,

$$\mathrm{Pe} = \frac{H\,\bar{u}}{\kappa}\ , \tag{12}$$

where H is the height of the plug and $\bar{u}$ the average gas segregation speed. Since the diffusivity of porous magma is small, $\kappa \approx 10^{-6}\ \mathrm{m^2/s}$, and the gas percolation speed potentially large, $\bar{u} = 10^{-5} - 10^{-3}$ m/s, the Péclet number is large, $\mathrm{Pe} \approx 10^3 - 10^5$. The temperature distribution in the plug is thus dominated by the heat transport from degassing and also localized.

In Figure 2, we show four calculations of our mush column model with different maximum vesicularity at the surface (10, 15, 22, and 30%). These values are somewhat lower than observed in ejected lavas, because the eruptive process amplifies vesicularity. The pronounced power-law relationship between permeability and vesicularity [*Bai et al.*, 2010] leads to a rapid increase in gas segregation. As a consequence, high permeability and high gas flux create a hot mush profile with intermediate crystallinity, low density and low viscosity. In contrast, low permeability results in comparatively cool temperatures, high crystallinity and high density and viscosity. The emerging picture is one of hot, permeable pathways of mobile magma embedded in a less permeable plug of relatively stagnant crystalline mush.

To quantify the rheological transition between mobile and stagnant magma we use the critical Rayleigh number for thermally driven and gas-buoyancy driven convection in a mush body of the dimensions of the hypothesized Strombolian plug (L = 100 m). These Rayleigh numbers quantify the competition between buoyancy forces driving flow, and viscous resistance and thermal diffusion that both dampen flow:

$$Ra_T = \frac{\alpha \rho_c \Delta T L^3}{\eta_c \kappa} , \quad Ra_G = \frac{\phi_c \Delta \rho L^3}{\eta_c \kappa} , \tag{13}$$

with α the thermal expansivity, ρ_c, ϕ_c, and η_c the characteristic density, vesicularity and viscosity of the mush, ΔT the temperature difference between the magma and the surface, and $\Delta\rho$ the density contrast between gas and the magma mush. Fig. 3A shows viscosity as a function of crystal fraction and temperature (at $X_{\mathrm{H2O}}^{\mathrm{sat}} = 0.5$ wt%). We mark the rheological transition between the mobile and stagnant regimes at a critical Rayleigh number of ~1000 (see Fig. 3), which is where small perturbations begin to grow into convective motion [e.g., *Turcotte and Schubert*, 2014]. A temperature-dependent crystallization path taken from a 1D mush model (Fig. 2, $\phi_v^{\max} = 30\%$) indicates that magma along that evolution path remains mobile (>10^{12} Pa s) while crystal fraction remains below ~55% and above temperatures ~1060 ºC, consistent with observations of erupted HP lavas.

The 1D mush model does not consider the effect of stresses inside the plug and the deformational behavior they create. The stresses inside the hypothesized plug result from topography, gravity, tectonics, and from gas over-pressure related to gas segregation. To estimate the stress distribution inside the plug prior to failure, we consider a range of tensile strengths for the plug of 0.5–5 MPa, which is significantly weaker than solid rock (~15 MPa). Our mechanical model shows that stresses in the plug contribute to its propensity to tensile failure (Fig. 4B), because they imply a finite shear stress. Figures 4C-D compare the likelihood of failure in the presence (C) and absence (D) of the regional tectonic stress field. Without the tectonic stress field, failure would be most likely along the southern edge of the crater terrace, just underneath the volcanic summit, the Pizzo sopra la Fossa. When accounting for the extensional stress field, the locus of maximum shear stress magnitude shifts towards the NE and SW segments of the ellipse, directly underneath the craters where most normal eruptions are observed (see SI for robustness tests).

5. Discussion

5.1. Localization of gas flux governs plug behavior

Our 1D mush model shows that continuous degassing through the hypothesized Strombolian plug is likely accommodated through numerous, localized bubble pathways. The gas-heated channels provide conduits for fast, localized degassing, whereas gas percolation occurs at much slower rates in the remaining mush body. The spacing of these channels depends primarily on the compaction length in the mush, which is itself variable but likely on the order of tens of meters. We suggest that passive degassing distributed across the crater terrace represents Darcy flux of gas through the cooler, stagnant portion of the mush plug. Puffing from eruptive vents and fumaroles may instead be related to comparatively fast, localized degassing along hot conduits, which is consistent with puffing being concentrated at the central vent where temperatures are highest [*Landi et al.*, 2011].

Localization of gas flux is consequential not only for temperature and gas flux, but also for the mechanical behavior of the plug. More specifically, our analysis shows that the magma in gas-heated channels could be eruptible, while magma in the cold portions of the mush plug is less mobile. According to our model, the eruption temperature of samples is hence more indicative of the magnitude of gas flux required to keep magma mobile than of the depth from which magma is erupted (see Fig. 2E–F). HP magma is derived from some range of pressures [*Taddeucci et al.*, 2012b] but only a narrow range of temperatures – at most $T = 1100 - 1180°C$ [*Landi et al.*, 2011]. We interpret the small variability in eruption temperatures as evidence that HP magmas may originate at various depths within gas-flushed conduits with near isothermal conditions. The significant rheological differences between magma that is hydrated and warm with intermediate crystallinity compared to magma that is dry, cool and highly crystalline leads to a dynamic selection of locations from which magma can be erupted and could explain why erupted lavas at Stromboli have rather homogeneous properties. Our model hence implies a close connection between continuous degassing and normal eruptions, which is consistent with observations showing that the repose time at a given vent is inversely correlated with the intra-eruptive gas flux [*Colò et al.*, 2010], and that eruption frequency and magnitude increase with the overall gas flux [*Taddeucci et al.*, 2013].

5.2. Normal eruptions may be the surface expression of tensile failure in the volcanic plug

Our results show that gas over-pressure in combination with a finite stress field make Griffith failure in the volcanic plug likely (see Figure 4B). In isolation, the two contributing factors bring the plug close to failure but we only expect failure for a small portion of the parameter space. For example, Figure 3B compares tensile strength to gas over-pressures corresponding to compaction lengths of 5–50 m. The pressure difference between mush and gas only grows sufficiently large to fracture the mush for compaction lengths >20 m, and for a magma strength of <1.3 MPa (Fig. 3B, cross-hatched). At gas fractions of 20–30% the viscosity required to reach such compaction lengths is 10^{10}–10^{12} Pas, which is not unreasonable but somewhat stiffer than predicted for the hot degassing conduits, where normal eruptions may be rooted. Similarly, when considering only tectonic stresses, the mean normal stress at the base of the plug tends to be compressive (see Figure 4B) unless we assume strongly extensional tectonic stress.

The likely possibility of tensile failure in the NE and SW segments of the plug leads us to suggest that normal eruptions may represent the surface expression of failure at depth and failure-facilitated ascent of gas pulses along hot conduits established by continuous degassing. This interpretation of normal eruptions is compatible with recent results from pyroclast-tracking velocimetry studies that decompose each normal explosion into a sequence of individual, concatenated ejection pulses [*Gaudin et al.*, 2014]. These pulses are thought to indicate rapid ejection of a sequence of gas pockets and entrained magma batches. Similar processes are also observed in analogue laboratory experiments of outgassing from particle-rich suspensions [*Oppenheimer et al.*, 2015]. Previous analysis suggests that tensile failure at the head of a buoyant pulse of pore fluid can speed up its velocity by several orders of magnitude [*Connolly and Podladchikov*, 2007; *Keller et al.*, 2013]. This effect would be amplified at Stromboli by the continuous expansion of accelerated gas pulses. While modeling failure propagation is beyond the scope of this model, a failure-based explanation for normal eruptions could explain observed rise speeds of gas pulses of up to 100 m/s [e.g., *Harris and Ripepe*, 2007a; *Patrick et al.*, 2007; *Taddeucci et al.*, 2012a, 2014], which are notoriously difficult to explain in models where a gas slug ascends through a magma-filled conduit by linear viscous flow only.

6. Conclusions

The goal of this paper is to generalize the slug model for Strombolian activity by considering the dynamic interactions between the three phases, gas, melt and crystals, present in the shallow plumbing system. Our three-phase framework posits the existence of a porous plug beneath the entire crater terrace, and links the different degassing regimes observed on the surface to the different modes of gas percolation. We find that conduits of localized gas flux may emerge dynamically from three-phase interactions, which could explain the shifting locations of active vents on the crater terrace [*Harris and Ripepe*, 2007b]. We propose that normal eruptions may be the surface expression of tensile failure of the plug, facilitated by gas-overpressures arising from gas percolation through the plug in combination with extensional tectonic stress. A fracture-based mechanism governing normal activity may help explain the rapid eruption speeds observed, as well as providing a possible source mechanism for VLP signals. We emphasize that both the slug and the plug model relate normal Strombolian activity to the exsolution and ascent of gas, but differ in the mechanism by which gas is driving eruptive activity. We conclude that while more work is needed to refine the plug model, it makes progress towards an integrated three-phase understanding of basaltic volcanism by accounting for both fracture and flow in the plumbing system.

Acknowledgements

The data used in this study have been assembled from the published literature cited in the manuscript. The script used to compute the mush column model (Fig. 2) and benchmark results from our 3D computations are available upon request from JS (email: jsuckale@stanford.edu). We acknowledge support from two GSA student-research grants awarded to JS and IBB, the AXA Research Fund awarded to KVC and by the AFOSR Computational Mathematics grant FA9550-10-1-0229, the Alfred P. Sloan foundation, and the Director, Office of Science, Computational and Technology Research, U.S. Department of Energy under Contract No. DE-AC02-05CH11231.

References

Agostini, C., a. Fortunati, F. Arzilli, P. Landi, and M. R. Carroll (2013), Kinetics of crystal evolution as a probe to magmatism at Stromboli (Aeolian Archipelago, Italy), *Geochim. Cosmochim. Acta*, *110*, 135–151, doi:10.1016/j.gca.2013.02.027.

Aharonov, E., J. A. Whitehead, P. B. Kelemen, and M. Spiegelman (1995), Channeling instability of upwelling melt in the mantle, *J. Geophys. Res.*, *100*, 20433–20450.

Allard, P., J. Carbonnelle, N. Métrich, H. Loyer, and P. Zettwoog (1994a), Sulphur output and magma degassing budget of Stromboli volcano, *Nature*, *368*(6469), 326–330.

Allard, P., J. Carbonnelle, N. Métrich, H. Loyer, and P. Zettwoog (1994b), Sulphur output and magma degassing budget of Stromboli volcano, *Nature*, *368*(6469), 326–330, doi:10.1038/368326a0.

Arzi, A. A. (1978), Critical phenomena in the rheology of partially melted rocks, *Tectonophysics*, *44*(1–4), 173–184.

Bai, L., D. R. Baker, and R. J. Hill (2010), Permeability of vesicular Stromboli basaltic glass: Lattice Boltzmann simulations and laboratory measurements, *J. Geophys. Res.*, *115*(B7), 1–16, doi:10.1029/2009JB007047.

Ballestracci, R. (1982), Self-potential survey near the craters of Stromboli volcano (Italy). Inference for internal structure and eruption mechanism, *Bull. Volcanol.*, *45*(4), 349–365.

Barberi, F., M. Rosi, and A. Sodi (1993), Volcanic hazard assessment at Stromboli based on review of historical data, *Acta Volcanol.*, *3*, 173–187.

Bertagnini, A., N. Métrich, P. Landi, and M. Rosi (2003), Stromboli volcano (Aeolian

Archipelago, Italy): an open window on the deep-feeding system of a steady state basaltic volcano, *J. Geophys. Res.*, *108*(B7), 2336–2350.

Blackburn, E. A., L. Wilson, and R. S. J. Sparks (1976), Mechanisms and dynamics of strombolian activity, *J. Geol. Soc.*, *132*(4), 429–440.

Calvari, S., L. Spampinato, L. Lodato, A. J. L. Harris, M. R. Patrick, J. Dehn, M. R. Burton, and D. Andronico (2005), Chronology and complex volcanic processes during the 2002-2003 flank eruption at Stromboli volcano (Italy) reconstructed from direct observations and surveys with a handheld thermal camera, *J. Geophys. Res. B Solid Earth*, *110*(2), 1–23, doi:10.1029/2004JB003129.

Carbone, D., L. Zuccarello, P. Montalto, and H. Rymer (2012), New geophysical insight into the dynamics of Stromboli volcano (Italy), *Gondwana Res.*, *22*(1), 290–299, doi:10.1016/j.gr.2011.09.007.

Caricchi, L., L. Burlini, P. Ulmer, T. Gerya, M. Vassalli, and P. Papale (2007), Non-Newtonian rheology of crystal-bearing magmas and implications for magma ascent dynamics, *Earth Planet. Sci. Lett.*, *264*(3–4), 402–419.

Chevalier, C., A. Lindner, and E. Clément (2008), Destabilization of a Saffman-Taylor fingerlike pattern in a granular suspension, *J. Nonnewton. Fluid Mech.*, *99*(4), doi:10.1103/PhysRevLett.99.174501.

Chevalier, C., A. Lindner, M. Leroux, and E. Clément (2009), Morphodynamics during air injection into a confined granular suspension, *J. Nonnewton. Fluid Mech.*, *158*, 63–72, doi:10.1016/j.jnnfm.2008.07.007.

Chouet, B., P. Dawson, T. Ohminato, M. Martini, G. Saccorotti, F. Giudicepietro, G. De Luca,

G. Milana, and R. Scarpa (2003), Source mechanisms of explosions at Stromboli Volcano, Italy, determined from moment-tensor inversions of very-long-period data, *J. Geophys. Res*, *108*(B1), 2019.

Cigolini, C., M. Laiolo, and S. Bertolino (2008), Probing Stromboli volcano from the mantle to paroxysmal eruptions, *Geol. Soc. London, Spec. Publ.*, *304*(1), 33–70.

Cigolini, C., M. Laiolo, and D. Coppola (2015), Revisiting the last major eruptions at Stromboli volcano: inferences on the role of volatiles during magma storage and decompression, in *Geological Society Special Publication*, vol. 410, pp. 143–177, Universita degli Studi di Torino, Torino, Italy.

Colò, L., M. Ripepe, D. R. Baker, and M. Polacci (2010), Magma vesiculation and infrasonic activity at Stromboli open conduit volcano, *Earth Planet. Sci. Lett.*, *292*(3–4), 274–280, doi:10.1016/j.epsl.2010.01.018.

Connolly, J. A. D., and Y. Y. Podladchikov (2007), Decompaction weakening and channeling instability in ductile porous media: Implications for asthenospheric melt segregation, *J. Geophys. Res.*, *112*(B10205), B10205.

Conte, A. M., C. Perinelli, and R. Trigila (2006), Cooling kinetics experiments on different Stromboli lavas: Effects on crystal morphologies and phases composition, *J. Volcanol. Geotherm. Res.*, *155*(3–4), 179–200, doi:10.1016/j.jvolgeores.2006.03.025.

Finizola, A., F. Sortino, J. F. Lenat, M. Aubert, M. Ripepe, and M. Valenza (2003), The summit hydrothermal system of Stromboli. New insights from self-potential, temperature, CO2 and fumarolic fluid measurements, with structural and monitoring implications, *Bull. Volcanol.*, *65*(7), 486–504.

Francalanci, L., S. Tommasini, and S. Conticelli (2004), The volcanic activity of Stromboli in the 1906-1998 AD period: mineralogical, geochemical and isotope data relevant to the understanding of the plumbing system, *J. Volcanol. Geotherm. Res.*, *131*(1--2), 179–211.

Francalanci, L., G. R. Davies, W. Lustenhouwer, S. Tommasini, P. R. D. Mason, and S. Conticelli (2005), Intra-grain Sr isotope evidence for crystal recycling and multiple magma reservoirs in the recent activity of Stromboli Volcano, Southern Italy, *J. Pet.*, *46*(10), 1997–2021.

Gaudin, D., J. Taddeucci, P. Scarlato, M. Moroni, C. Freda, M. Gaeta, and D. M. Palladino (2014), Pyroclast Tracking Velocimetry illuminates bomb ejection and explosion dynamics at Stromboli(Italy) and Yasur (Vanuatu) volcanoes, *J. Geophys. Res.*, *119*, 5384–5397, doi:10.1002/2014JB011096.Received.

Genco, R., and M. Ripepe (2010), Inflation-deflation cycles revealed by tilt and seismic records at Stromboli volcano, *Geophys. Res. Lett.*, *37*(12), 1–5, doi:10.1029/2010GL042925.

Gurioli, L., L. Colo', B. A. J., H. A. J. L., W. A., and M. Ripepe (2014), Dynamics of Strombolian explosions: Inferences from field and laboratory studies of erupted bombs from Stromboli volcano, *J. Geophys. Res. Solid Earth*, *119*, 319–345, doi:10.1002/2013JB010264.Received.

Harris, A., and M. Ripepe (2007a), Synergy of multiple geophysical approaches to unravel explosive eruption conduit and source dynamics - A case study from Stromboli, *Chemie der Erde - Geochemistry*, *67*(1), 1–35, doi:10.1016/j.chemer.2007.01.003.

Harris, A., and M. Ripepe (2007b), Temperature and dynamics of degassing at Stromboli, *J. Geophys. Res. Solid Earth*, *112*(3), 1–18, doi:10.1029/2006JB004393.

Harris, A. J. L., N. F. Stevens, A. J. H. Maciejewski, and P. J. Röllin (1996), Thermal evidence for linked vents at Stromboli, *Acta Volcanol.*, *8*, 57–62.

Holtzman, R., M. L. Szulczewski, and R. Juanes (2012), Capillary fracturing in granular media., *Phys. Rev. Lett.*, *108*(4), 180–189, doi:10.1103/PhysRevLett.108.264504.

Islam, A., S. Chevalier, and M. Sassi (2013), Experimental and numerical studies of CO$_2$ injection into water-saturated porous medium: capillary to viscous to fracture fingering phenomenon., *Energy Procedia*, *37*, 5511–5519, doi:10.1016/j.egypro.2013.06.471.

Katz, R. F. (2003), A new parameterization of hydrous mantle melting, *Geochemistry Geophys. Geosystems*, *4*(9), 1073.

Keller, T., and R. F. Katz (2016), The role of volatiles in reactive melt transport in the asthenosphere, *J. Petrol.*, *57*(6), 1073–1108.

Keller, T., D. A. May, and B. J. P. Kaus (2013), Numerical modeling of magma dynamics coupled to tectonic deformation of lithosphere and crust, *Geophys. J. Int.*, *196*.

Kirchdörfer, M. (1999), Analysis and quasistatic FE modeling of long period impulsive events associated with explosions at Stromboli volcano (Italy), *Ann. Geophys.*, *42*(3), 379–390.

Knudsen, H. A., B. Sandnes, E. G. Flekkøy, and K. J. Måløy (2008), Granular labyrinth structures in confined geometries, *Phys. Rev. E*, *77*(21301), doi:10.1103/PhysRevE.77.021301.

Landi, P., N. Métrich, A. Bertagnini, and M. Rosi (2004), Dynamics of magma mixing and degassing recorded in plagioclase at Stromboli (Aeolian Archipelago, Italy), *Contrib. to Mineral. Petrol.*, *147*(2), 213–227, doi:10.1007/s00410-004-0555-5.

Landi, P., E. Marchetti, S. La Felice, M. Ripepe, and M. Rosi (2011), Integrated petrochemical and geophysical data reveals thermal distribution of the feeding conduits at Stromboli volcano, Italy, *Geophys. Res. Lett.*, *38*(8), 1–6, doi:10.1029/2010GL046296.

Liu, A. J., and S. R. Nagel (n.d.), The jamming transition and the marginally jammed solid, *Annu. Rev. Condens. Matter Phys.*, *1*, 347–369, doi:10.1146/annurev-conmatphys-070909-104045.

Majmudar, T. S., and R. P. Behringer (2005), Contact force measurements and stress-induced anisotropy in granular materials., *Nature*, *435*(7045), 1079–1082, doi:10.1038/nature03805.

Marsh, B. D. (2000), Magma Chambers, in *Encyclopedia of Volcanoes*, pp. 191–217, Academic Press.

De Martino, S., A. Errico, M. Palo, and G. B. Cimini (2012), Explosion swarms at Stromboli volcano: A proxy for nonequilibrium conditions in the shallow plumbing system, *Geochem., Geophys. Geosys.*, *13*(3), 1–16, doi:10.1029/2011GC003949.

La Spina, G., M. Burton, and M. de' Michieli Vitturi (2015), Temperature evolution during magma ascent in basaltic effusive eruptions: A numerical application to Stromboli volcano, *Earth Planet. Sci. Lett*., 426, 89-100, doi: 10.1016/j.epsl.2015.06.015.

McKenzie, D. (1984), The Generation and Compaction of Partially Molten Rock, *J. Petrol.*, *25*(3), 713–765.

Métrich, N., A. Bertagnini, P. Landi, and M. Rosi (2001), Crystallization driven by decompression and water loss at Stromboli volcano (Aeolian Islands, Italy), *J. Petrol.*, *42*(8), 1471–1490, doi:10.1093/petrology/42.8.1471.

Métrich, N., A. Bertagnini, and A. Di Muro (2009), Conditions of magma storage, degassing and ascent at Stromboli: New insights into the volcano plumbing system with inferences on the eruptive dynamics, *J. Petrol.*, *51*(3), 603–626, doi:10.1093/petrology/egp083.

van der Molen, I., and M. S. Paterson (1979), Experimental deformation of partially-melted granite, *Cont. Miner. Petr.*, *70*(3), 299–318.

Montone, P., M. T. Mariucci, and S. Pierdominici (2012), The Italian present-day stress map, *Geophys. J. Int.*, *189*(2), 705–716.

Oppenheimer, J., A. C. Rust, K. V. Cashman, and B. Sandnes (2015), Gas migration regimes and outgassing in particle-rich suspensions, *Front. Phys.*, *3*(August), 1–13, doi:10.3389/fphy.2015.00060.

Patrick, M. R., A. J. L. Harris, M. Ripepe, J. Dehn, D. A. Rothery, and S. Calvari (2007), Strombolian explosive styles and source conditions: insights from thermal (FLIR) video, *Bull. Volcanol.*, *69*(7), 769–784.

Peraire, J., and P. Persson (2011), High-Order Discontinuous Galerkin Methods for CFD, in *Adaptive high-order methods in computational fluid dynamics*, pp. 119–152, World Sci. Publ.

Persson, P.-O., and G. Strang (2004), A simple mesh generator in matlab, *SIAM Rev.*, *46*(2), 329–345.

Pistone, M., L. Caricchi, P. Ulmer, E. Reusser, and P. Ardia (2013), Rheology of volatile-bearing crystal mushes: Mobilization vs. viscous death, *Chem. Geol.*, *345*, 16–39, doi:10.1016/j.chemgeo.2013.02.007.

Renner, J., B. Evans, and G. Hirth (2000a), On the rheologically critical melt fraction, *Earth Planet. Sci. Lett.*, *181*(4), 585–594.

Renner, J., B. Evans, and G. Hirth (2000b), On the rheologically critical melt fraction, *Earth Planet. Sci. Lett.*, *181*(4), 585–594, doi:10.1016/S0012-821X(00)00222-3.

Ripepe, M., A. J. L. Harris, and E. Marchetti (2005a), Coupled thermal oscillations in explosive activity at different craters of Stromboli volcano, *Geophys. Res. Lett.*, *32*(17), 1–4, doi:10.1029/2005GL022711.

Ripepe, M., E. Marchetti, G. Ulivieri, A. Harris, J. Dehn, M. Burton, T. Caltabiano, and G. Salerno (2005b), Effusive to explosive transition during the 2003 eruption of Stromboli volcano, *Geology*, *33*(5), 341–344, doi:10.1130/G21173.1.

Ripepe, M., E. Marchetti, and G. Ulivieri (2007), Infrasonic monitoring at Stromboli volcano during the 2003 effusive eruption: Insights on the explosive and degassing process of an open conduit system, *J. Geophys. Res.*, *112*(B9), B09207.

Saffman, P. G., and G. Taylor (1958), The Penetration of a Fluid into a Porous Medium or Hele-Shaw Cell Containing a More Viscous Liquid, *Proc. R. Soc. A Math. Phys. Eng. Sci.*, *245*(1242), 312–329.

Sandnes, B., E. G. Flekkøy, H. a. Knudsen, K. J. Måløy, and H. See (2011), Patterns and flow in frictional fluid dynamics, *Nat. Commun.*, *2*, 288, doi:10.1038/ncomms1289.

Settle, M., and T. R. McGetchin (1980), Statistical analysis of persistent explosive activity at Stromboli, 1971: Implications for eruption prediction, *J. Volcanol. Geotherm. Res.*, *8*, 45–58.

Shin, H., and J. C. Santamarina (2010), Fluid-driven fractures in uncemented sediments: underlying particle-level processes, *Earth Planet. Sci. Lett.*, *299*, 180–189, doi:10.1016/j.epsl.2010.08.033.

Skempton, A. W. (1960), Effective stress in soils, concrete and rocks, in *Proc Conf Pore Pressure and Suction in Soils*, pp. 4–16, Butterworths, London, UK.

Spiegelman, M., P. B. Kelemen, and E. Aharonov (2001), Causes and consequences of flow organization during melt transport: The reaction infiltration instability in compactible media, *J. Geophys. Res.*, *106*(B2), 2061–2077.

Stevenson, D. J. (1989), Spontaneous small-scale melt segregation in partial melts undergoing deformation, *Geophys. Res. Lett.*, *16*, 1067–1070.

Taddeucci, J., P. Scarlato, a. Capponi, E. Del Bello, C. Cimarelli, D. M. Palladino, and U. Kueppers (2012a), High-speed imaging of Strombolian explosions: The ejection velocity of pyroclasts, *Geophys. Res. Lett.*, *39*(2), 1–6, doi:10.1029/2011GL050404.

Taddeucci, J., M. A. Alatorre-Ibargüengoitia, M. Moroni, L. Tornetta, A. Capponi, P. Scarlato, D. B. Dingwell, and D. De Rita (2012b), Physical parameterization of Strombolian eruptions via experimentally- validated modeling of high-speed observations, *Geophys. Res. Lett.*, *39*(16), 2–7, doi:10.1029/2012GL052772.

Taddeucci, J., D. M. Palladino, G. Sottili, D. Bernini, D. Andronico, and a. Cristaldi (2013), Linked frequency and intensity of persistent volcanic activity at Stromboli (Italy), *Geophys. Res. Lett.*, *40*(13), 3384–3388, doi:10.1002/grl.50652.

Taddeucci, J., J. Sesterhenn, P. Scarlato, K. Stampka, E. Del Bello, J. J. Pena Fernandez, and D.

Gaudin (2014), High-speed imaging, acoustic features, and aeroacoustic computations of jet noise from Strombolian (and Vulcanian) explosions, *Geophys. Res. Lett.*, 3096–3102, doi:10.1002/2014GL059925.

Tibaldi, A., C. Corazzato, T. Apuani, and A. Cancelli (2003), Deformation at Stromboli volcano (Italy) revealed by rock mechanics and structural geology, *Tectonophys.*, 361(3–4), 187–204, doi:10.1016/S0040195102005899.

Tordesillas, A. (2007), Force chain buckling, unjamming transitions and shear banding in dense granular assemblies, *Philos. Mag.*, *87*(32), 4987–5016, doi:10.1080/14786430701594848.

Turcotte, D. L., and G. Schubert (2014), *Geodynamics*, book, Cambridge University Press.

Varas, G., V. Vidal, and J. C. Géminard (2010), Morphology of air invasion in an immersed granular layer., *Phys. Rev. E*, *83*(7), doi:10.1103/physreve.83.061302.

Varas, G., J. C. Géminard, and V. Vidal (2013), Air invasion in a granular layer immersed in a fluid: morphology and dynamics., *Granul. Matter*, *15*, 801–810, doi:10.1007/s10035-013-0435-7.

Vergniolle, S., and M. Mangan (2000), Hawaiian and Strombolian eruptions, in *Encyclopedia of Volcanoes*, edited by H. Sigurdsson, pp. 447–462, Academic Press.

Washington, H. S. (1917), Persistence of vents at Stromboli and its bearing on volcanic mechanism, *Bull. Geol. Soc. Am.*, *28*, 249–278.

Wielandt, E., and T. Forbriger (1999), Near-field seismic displacement and tilt associated with the explosive activity of Stromboli, *Ann. di Geofis.*, *42*, 407–416.

Figure captions

Figure 1. **A:** The slug model relates normal eruptions to the burst of periodically rising gas slugs (white) in a fixed conduit filled with liquid magma (red). **B:** The plug model captures the simplified dynamics of a mush plug consisting of HP magma beneath the entire crater terrace. Crystals are shown in grey and bubbles in white. The background color illustrates the transition from fluid-like behavior (red) to solid-like behavior (black) based on temperature and crystal content. Gas flux in the plug localizes in hot, gas-rich and crystal-poor pathways as compared to the surrounding plug. Fast gas pulses accommodated by tensile failure (yellow) follow these pathways to feed normal eruptive activity.

Figure 2. Results of the thermally coupled degassing model in a 1D mush column. Profiles with depth of: **A** gas fraction; **B** crystal and melt fractions; **C** mush density; **D** gas segregation speed; **E** temperature, with the magma solidus and liquidus (dotted); **F** mush viscosity, with the approximate regime boundary between mobile and stagnant mush (dotted). Line colors indicate different levels of final vesicularity contrasting low with high gas flux environments; the former creates conditions for passive degassing through a cooler, highly crystalline, stagnant mush plug; the latter for active degassing through gas-heated, lower crystallinity conduits of mobile magma.

Figure 3. Integrated scaling analysis of thermal and mechanical state of the volcanic plug at Stromboli: **A:** Mush viscosity plotted against crystal fraction and temperature. Rheological transition between mobile and stagnant regimes (black solid and dashed) corresponding to critical Rayleigh number for thermal and gas-buoyancy driven convection on the length scale of 100 m. Crystallinity as a function of temperature (dotted) taken from 1D model results (Fig. 2,

$\phi_v^{\max} = 30\%$). **B:** Characteristic gas over-pressure calculated as a function of mush viscosity and gas fraction. Over-pressure at compaction lengths of 5–50 m (black contours), and tensile strength of 0.5–5 MPa (white contours). Tensile failure driven by gas over-pressure predicted for zone of overlapping patterns. 1D model results of viscosity and gas fraction for final vesicularity of 15–25% (dotted, cf. Fig. 2).

Figure 4. **A:** Cross-section through the computational mesh used to model Stromboli. The NE–SW oriented elliptical magmatic body is aligned with the main direction of normal faulting along the Panarea-Stromboli alignment (grey dashed line) implying that the least compressive stress, σ_3, is oriented NW–SE. The intermediate principle stress, σ_2, is oriented NE–SW and the most compressive stress, σ_1, is vertical. The liquid melt at large depth exerts magmastatic pressure on the walls of the plumbing system but has zero shear strength. **B:** Griffith criterion for tensile failure and stress state at the center (grey), and at either end of the crater terrace (black) when neglecting gas over-pressure (dashed circles) and when assuming a gas over-pressure of 0.25 MPa (solid line circles), which corresponds to an interconnected gas pulse of $\delta = 10\,\text{m}$. The axes are mean normal stress and effective stress defined as the square root of the second invariant of the deviatoric stress tensor. **C:** Locations where tensile failure is most likely to occur at 285 m below the crater terrace, the approximate source depth of the VLP signal [*Chouet et al.*, 2003]. The black dots represent vent locations mapped for ten years between August 1995 and June 2004 [*Harris and Ripepe*, 2007b].

Figure 1:

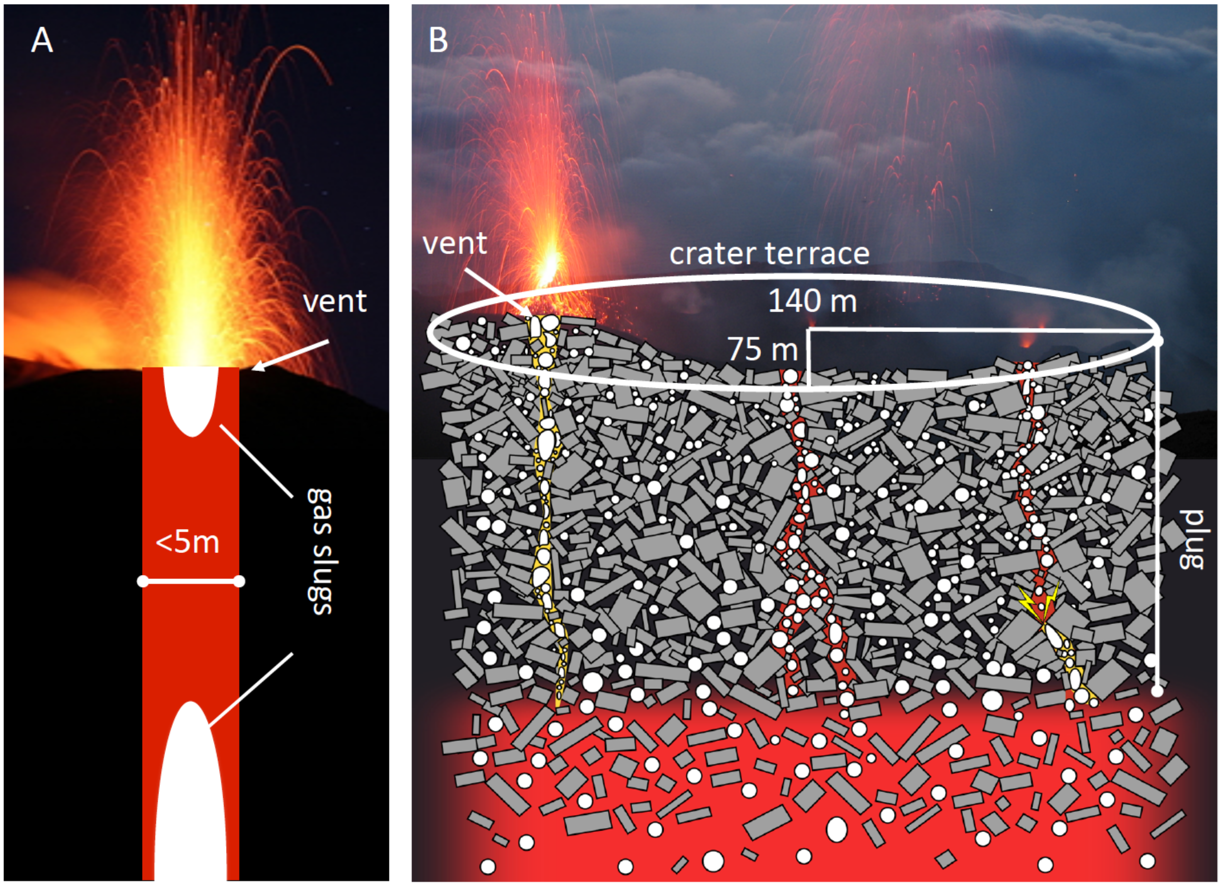

Figure 2:

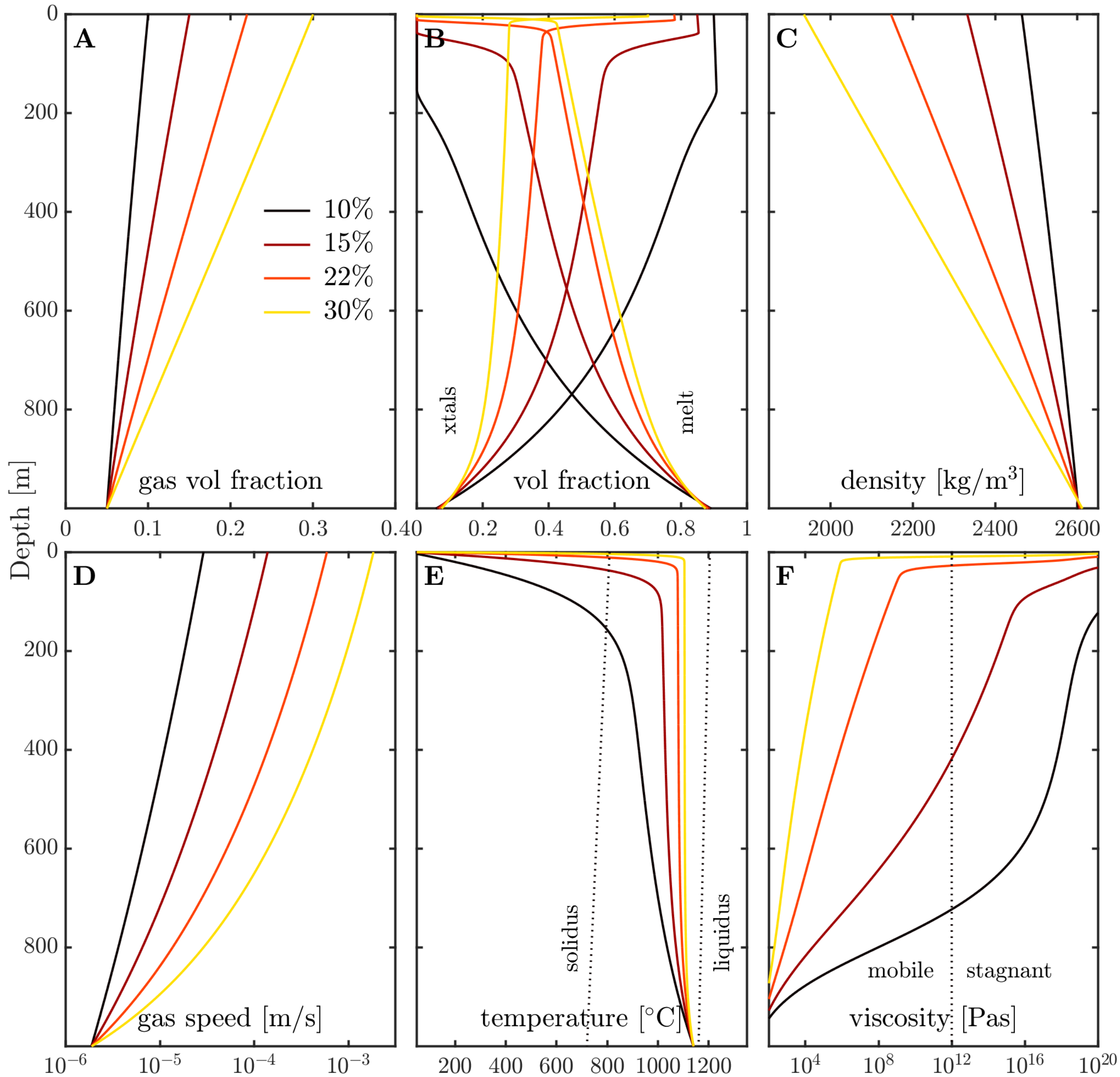
A
B
C
D
E
F
Depth [m]
gas vol fraction
vol fraction
density [kg/m^3]
gas speed [m/s]
temperature [°C]
viscosity [Pas]
10%
15%
22%
30%
xtals
melt
solidus
liquidus
mobile
stagnant

Figure 3:

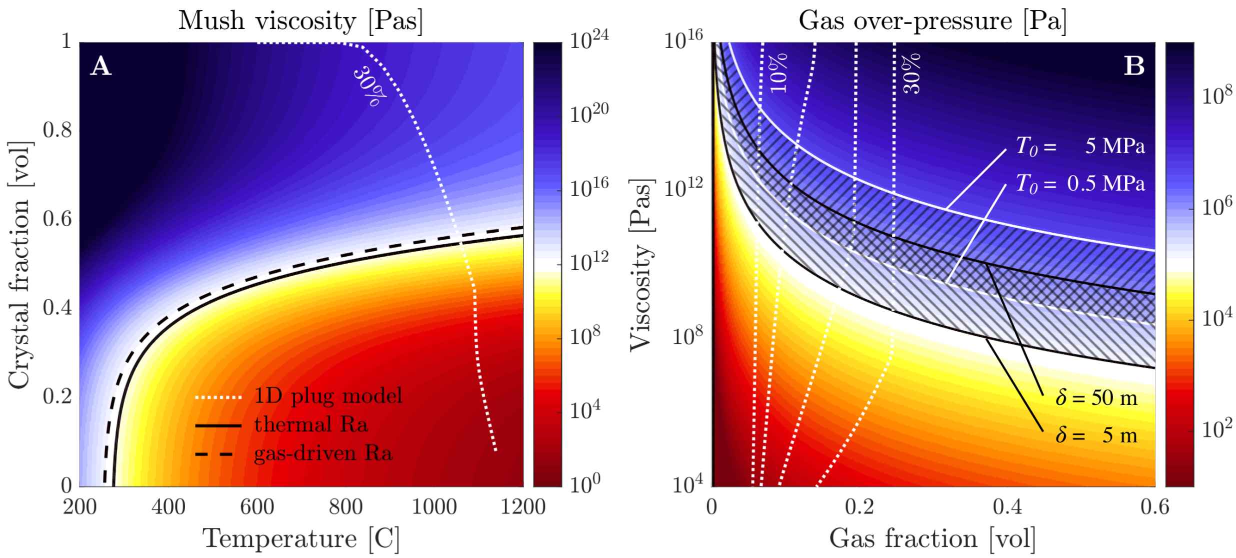
Mush viscosity [Pas]
A
30%
Crystal fraction [vol]
Temperature [C]
1D plug model
thermal Ra
gas-driven Ra
Gas over-pressure [Pa]
B
10%
30%
T_0 = 5 MPa
T_0 = 0.5 MPa
δ = 50 m
δ = 5 m
Viscosity [Pas]
Gas fraction [vol]

Figure 4:

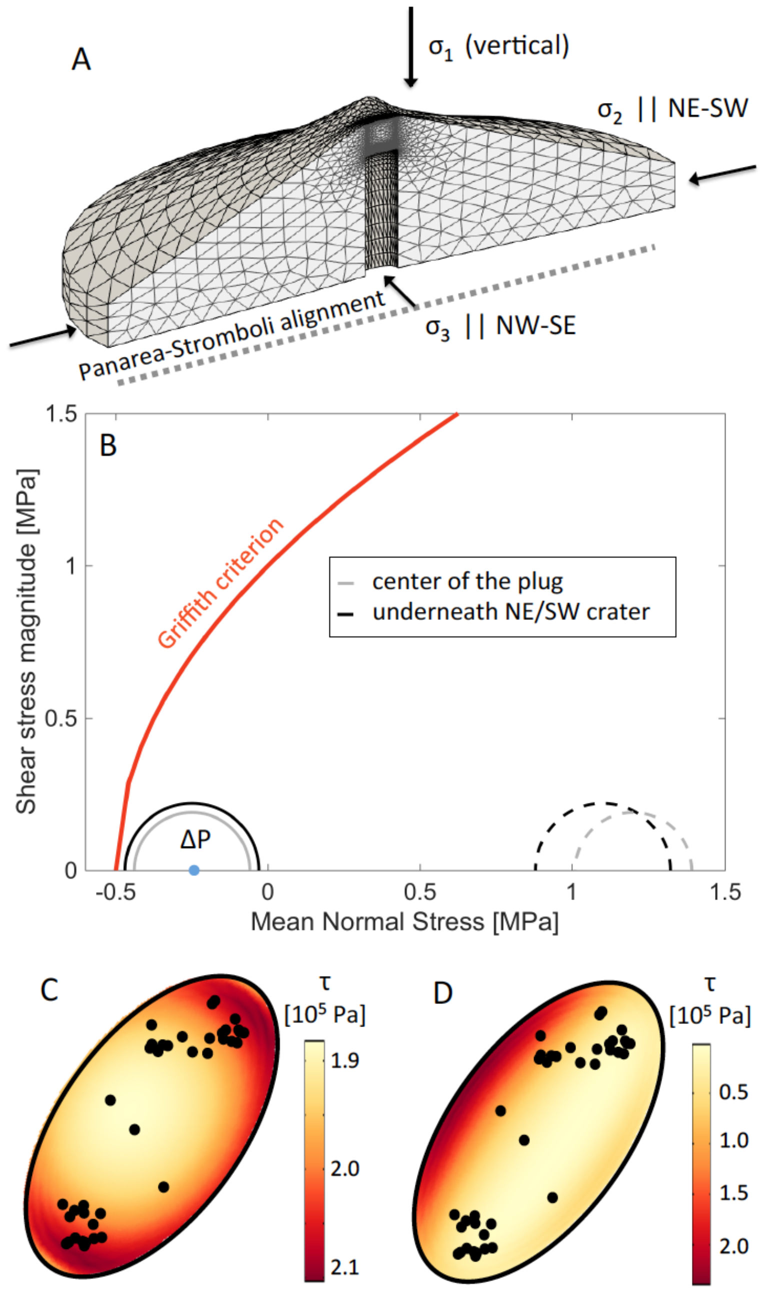
A
σ1 (vertical)
σ2 || NE-SW
σ3 || NW-SE
Panarea-Stromboli alignment
B
Griffith criterion
center of the plug
underneath NE/SW crater
ΔP
Shear stress magnitude [MPa]
Mean Normal Stress [MPa]
1.5
1
0.5
0
-0.5
0
0.5
1
1.5
C
τ
[10⁵ Pa]
1.9
2.0
2.1
D
τ
[10⁵ Pa]
0.5
1.0
1.5
2.0